Preparation of a hydrophobic cerium oxide nanoparticle coating with polymer binder via a facile solution route

Sumaira Yasmeen[a], Mohammad Rizwan Khan[a], Kiho Park[b], Yunshik Cho[b], Jang Wook Choi[b], Hyoung-Seok Moon[c], Han-Bo-Ram Lee[a,*]

[a] *Department of Materials Science & Engineering, Incheon National University, Incheon, South Korea*
[b] *School of Chemical and Biological Engineering and Institute of Chemical Processes, Seoul National University, Seoul, South Korea*
[c] *Energy Plant R&D Group, Korea Institute of Industrial Technology, Busan, South Korea*

A B S T R A C T

In this work, cerium oxide (CeO$_2$) nanoparticles (NPs) were synthesized using a facile, low temperature solution process and coated using spin coating and spray coating approaches, for the fabrication of a hydrophobic surface coating. Silicon wafer (Si) substrates coated with CeO$_2$ NPs exhibited excellent hydrophobic behavior, but poor adhesion of the NPs to the substrate was observed - likely due to the low surface polarity of CeO$_2$ NPs. Polyacrylic acid (PAA) was introduced as an adhesion promoter to improve NP surface characteristics and obtain an adherent and cohesive coating. Slight polarity tuning and binder inclusion significantly enhanced the binding capability of the NPs as determined by peel-off measurements. The superior mechanical properties of NP coatings were attributed to the incorporation of PAA in the polymeric network. It improves inter-particle and particle-substrate secondary interactions, ultimately aiding NP cohesion and adhesion when deposited onto the Si substrate. The adhesive and hydrophobic properties of CeO$_2$ NP coatings were maintained upon exposure to high temperatures, and the coatings are transparent as well, making them suitable for various applications, such as cookware, glass coating and technology components.

1. Introduction

Organic materials like polytetrafluoroethylene (PTFE), polypropylene, and fluorosilane have been extensively employed as hydrophobic coatings due to their low surface energy, cost-effective production and corrosion resistance [1,2]. However, organic coatings are unfit for harsh environmental conditions due to their low wear resistance, inherently poor mechanical durability, and poor thermal stability. For instance, repetitive strain on an organic layer can cause cracks that provide paths for easy water penetration, resulting in the failure of the hydrophobic coating. In addition, though polymers have hydrophobic properties due to their low surface energy, the dehydrogenation reaction, in which the bond between carbon and hydrogen is broken at a temperature of 200–300 °C, is a considerable limitation to their use as hydrophobic coatings [3].

Various studies have explored the hydrophobicity of inorganic metal oxides which exhibit better mechanical properties than organic materials. However, the major drawback of these coatings is that their hydrophobic characteristics are lost upon exposure to ultraviolet (UV)

light, and at high temperatures. Rare earth oxides (REOs) have gained significant attention in the last few years, owing to their intrinsic hydrophobicity [4–6]. Due to their unique properties, the use of REOs as hydrophobic surfaces has been widely explored for various applications, ranging from industrial machinery to houseware [2,3,6]. Recently, Azimi et al. reported that REOs possess intrinsic hydrophobicity due to their distinct electronic configuration and excellent thermal stability under robust environments [7]. REOs exhibit an outermost $5s^2p^6$ orbital filled with electrons which completely shield the empty 4f orbital, resulting in weak polarity. Therefore, when in contact, there is no interaction between the outer orbital electrons and water, and due to the surface tension of the water, the contact angle (CA) drops to more than 90° [8,9]. Due to this unique electronic structure, REOs can maintain stable hydrophobicity even at high temperatures, are relatively resistant to heat, and exhibit excellent durability as ceramic materials [10]. Additionally, some REOs such as cerium oxide (CeO$_2$) (the REO used in this study), are inexpensive and can reduce manufacturing costs [11].

In our previous study, the preparation of a hydrophobic surface

---

from a thin REO film, using atomic layer deposition (ALD), was investigated [12]. Results confirmed the thermal stability [13] of the film at high temperatures and demonstrated the production of a thin and uniform hydrophobic surface. However, ALD has limited applications as it is a relatively expensive and complicated process. Other studies have employed different techniques to deposit thin REO films, such as atmospheric plasma spraying [14], high velocity oxy-fuel (HVOF) thermal spraying [15], sputtering [8] and cathodic electrodeposition [16]. However, all of these coating methods are expensive and involve complex procedures. Furthermore, a recent review article on transparent superhydrophobic surfaces indicated certain key issues in the existing research [17]. Moreover, they suggested some key directions for effectively closing the existing gap in superhydrophobic transparent coating research. These recommendations included focusing on improving the interfacial adhesion with NPs films, mechanical testing for substrate-film adhesion, and producing robust hydrophobic NPs films that have high mechanical adhesion with the substrate, possess superior hydrophobic properties, and are transparent in nature. Therefore, in this study we used a comparatively facile and inexpensive spin and spray coating method to prepare hydrophobic CeO_2 thin films, considering these existing key issues.

Whilst spin coating is an effective technique for obtaining 2D films, spray coating is more effective for coating 3D materials. However, spray coating using nanoparticle (NP) solutions is ineffective, as good adhesion with the substrate cannot be obtained. Spray-coated thin films generally have poor adhesion with the substrate due to weak van der Waals forces between the NPs and the substrate [18]. Pretreatments that intentionally roughen the surface of the substrate to improve adhesion have been widely used, but are not appropriate for sensitive and fragile substrates where physical damage to the substrate may occur [19,20]. Alternative approaches to improving adhesion have been reported, wherein the incorporation of polymeric materials was found to improve adhesion between metal oxide powders used in the electrodes of lithium-ion batteries [21–27]. Polymeric materials such as polyacrylic acid (PAA), were incorporated as a binding material and were reported to have increased the mechanical and charging stability of the electrodes.

In this work, a facile and low-cost solution deposition coating process was developed to prepare CeO_2 NP films with PAA - an adhesion promoting agent. The incorporation of PAA in CeO_2 NP films was found to significantly improve its interfacial adhesion strength when spin and spray-coated onto a silicon wafer (Si) substrate. The surface morphologies, chemical compositions, wetting properties and interfacial adhesion strengths of the films were analyzed by field emission scanning electron microscopy (FE-SEM), transmission electron microscopy (TEM), energy dispersive spectroscopy (EDS), X-ray diffraction (XRD), water contact angle (WCA), and peel-off measurements, respectively. Results suggested that binder inclusion does not affect the hydrophobic characteristics of the CeO_2 coatings, but improves the adhesion of the coating to the substrate surface by increasing the interfacial adhesion. To the best of our knowledge, there are no other reports of hydrophobic coatings of CeO_2 NPs prepared via the described method, focusing on the interfacial adhesion of a CeO_2 coating on a substrate. The simple processing technique described, enables the coating to be applied to a wide range of substrates, irrespective of their complex structures. We believe that such a robust hydrophobic coating exhibits potential for many complex technological applications in the near future.

2. Experimental section

Nanoparticle synthesis High-purity cerium (III) nitrate hexahydrate (99 %) and PAA was purchased from Sigma-Aldrich. Sodium hydroxide was obtained from DC chemicals. Ethyl alcohol (99.9 %) was bought from Samchun Chemicals, and de-ionized water (DI) was produced in-house. P-type Si (001) wafer was used as substrates. All chemicals were used as received, without further modification. CeO_2 NPs

were synthesized using a simple non-hydrolytic solution process. In an illustrative experiment, cerium nitrate hexahydrate (0.06 M) was dissolved in ethanol at 120 °C under stirring. A solution of sodium hydroxide (0.10 M, in ethanol) was added gradually to the above solution and stirred for 2 h (~300–400 rpm) at 120 °C. The obtained solution was then allowed to cool to ambient temperature. The resultant particles were obtained in the form of a white precipitate, and washed five times with 200 mL of ethanol. The CeO_2 NPs were then dispersed in ethanol for further analysis. The whole process was carried out in air. The reaction occurs as follows: initially, Ce^{3+} ions are formed which react with the hydroxyl groups of the added NaOH to form $Ce(OH)_3$ (eq. (1)). Condensation then occurs, resulting in the formation of CeO_2 NPs (eq. (3)). The equations of the dissolution reactions are given below:

$$Ce^{3+} + 3OH^- \rightarrow Ce(OH)_3 \tag{1}$$

$$Ce(OH)_3 + OH \rightarrow Ce(OH)_4 \tag{2}$$

$$Ce(OH)_4 + \Delta T \rightarrow CeO_2 + 2H_2O \uparrow \tag{3}$$

The CeO_2 NP solution (10 mL) was combined with PAA (1 μg) and stirred for 20 min at 60 °C, to ensure homogeneity. PAA concentration varied from 0.01 to 1 wt %. The solutions containing PAA and CeO_2 NPs were sonicated for 45 min and then deposited via spray coating.

Coating methods Prior to spin coating, Si substrates were sequentially cleaned with acetone, ethanol, and DI water in an ultrasonic bath for 10 min, then dried using nitrogen (N_2) gas. The prepared CeO_2 NPs were spin coated on the cleaned substrate at 1000 rpm for one 60 s cycle, then sintered at 120 °C for 1 h to induce film formation. This process was repeated for a defined number of cycles to form CeO_2 NP films of varying thicknesses on the Si substrates. For spray coating, a home-built spray coating system with a computer interface and Wi-Fi connectivity was employed, as shown in Fig. S1. The CeO_2 NP solution was introduced by a dispenser through the inlet of the atomizer. Compressed N_2 gas was passed through a dust filter prior to the gas inlet. The pressure of the gas was maintained throughout the process of coating using a gas regulator. The solution flow rate and N_2 gas pressure were maintained at 2 mL/min and 15 psi, respectively. The distance between the substrate and the spray gun was maintained at 15 cm throughout the coating cycle, and the coating was conducted at ambient temperature.

Characterization The morphologies of the synthesized CeO_2 NPs were analyzed by FE-SEM (JEOL JSM-7800F, JEOL Ltd.) and TEM (JEM-ARM 200F, JEOL USA Inc.). The chemical composition of the product was evaluated by energy-dispersive X-ray spectroscopy (EDS). The crystal structure and phase purity of CeO_2 NPs were obtained by XRD (Cu Kα, λ = 1.54 Å, SmartLab, Rigaku). WCA was investigated via the sessile drop technique, using a contact angle analyzer (SDL200TEZD, FEMTOFAB) with DI water. WCA images were observed by a charge-coupled device video camera and an image analysis system. A water droplet of 2 μL was deposited onto the sample surface to measure the contact angle. A spectroscopic ellipsometer (Ellipso Technology Company, Spectroscopic Ellipsometer-SE-F) was used for thickness measurements. CeO_2 NPs were coated over a glass substrate to analyze the transparency of the films. Transmission spectra of the films were collected using Perkin Elmer Lambda 365 UV–Vis spectrometer.

For peeling tests, 3 M tape was attached to the top of the films, while one end of the tape was attached firmly to the support. The peeling strengths during detachment of the 3 M tape and adhesion force versus the detachment distance, were recorded on a high-precision micromechanical test instrument (QM100S, QMESYS, Korea).

3. Results and discussion

Fig. 1a and 1b shows TEM images of CeO_2 NPs synthesized with 0.03 and 0.06 M concentrations of cerium oxide precursor i.e. Ce
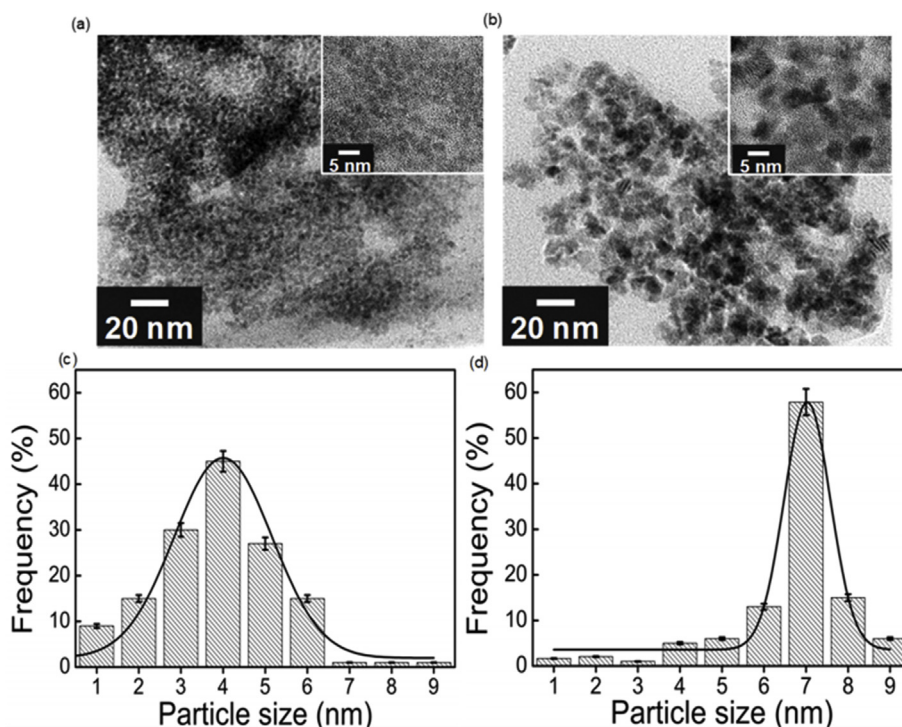
Fig. 1. Low and high (inset) resolutions TEM image of the CeO$_2$ NPs with different concentrations i.e. 0.0.3 M (a) and 0.06 M (b). Graph showing NPs distribution as a function of particles size for 0.03 M(c) and 0.06 M(d) concentrations, respectively.

(NO$_3$)$_3$.6H$_2$O, respectively. TEM images clearly confirmed the presence of dense and spherical CeO$_2$ NPs. The CeO$_2$ NPs prepared at a concentration of 0.06 M, exhibited larger particle size than the solution prepared at a concentration of 0.03 M. Fig. 1c and 1d shows the size distribution of the CeO$_2$ NPs with 0.03 M and 0.06 M, respectively. The solution prepared at a concentration of 0.03 M, accounts for 18 %, 36 %, and 22 % of the 3.7, 4.5 and 5.4 nm sized particles, respectively, as shown in Fig. 1c. The average particle size for the NPs prepared at 0.03 M was approximately 4 nm. The CeO$_2$ NPs prepared at concentrations of 0.06 M each account for 13 %, 57 %, and 15 % of the 6, 7, and 8 nm particles, respectively, with an average size of 7 nm, as shown in Fig. 1d. An increase in NP size was observed on increasing cerium oxide precursor concentrations. This is because higher precursor concentrations increase the number of growth species, in a fixed reaction volume, which results in an increase in the size of the NPs.

CeO$_2$ thin films were prepared using spin coating (20 cycles) and their thermal stability was observed by annealing at 200 °C for 4, 8, and 12 h. XRD analysis of the annealed films is shown in Fig. 2a. In Fig. 2a, the five XRD peaks were detected at 2θ angles of 28.4, 33, 47, 56, and 59° corresponding to (111), (200), (220), (311), and (222) peaks, respectively [18]. However, a relatively broad and weak intensity peak was observed when annealing was done for 4 h, while a narrow and strong intensity peak when annealing was done for 12 h. The average crystallite size of the NPs calculated using Scherer's equation were 6.67, 6.77, and 7.57 nm for the CeO$_2$ film annealed at 200 °C for 4, 8, and 12 h, respectively. The average crystallite size calculated was 7.52 ± 0.19 nm, and is in agreement with the average size obtained from the TEM images (i.e. 7 nm), thereby indicating no significant change in NP size during annealing. Surface morphologies of the spin-coated CeO$_2$ films were also confirmed using FE-SEM as shown in Fig. 2b. From the FE-SEM images, it was observed that CeO$_2$ NPs were deposited uniformly and densely. The chemical composition and distribution of the CeO$_2$ thin films were analyzed by EDS. A uniform distribution of Ce and O were detected in the film, indicating that CeO$_2$ NPs were successfully deposited onto the substrates.

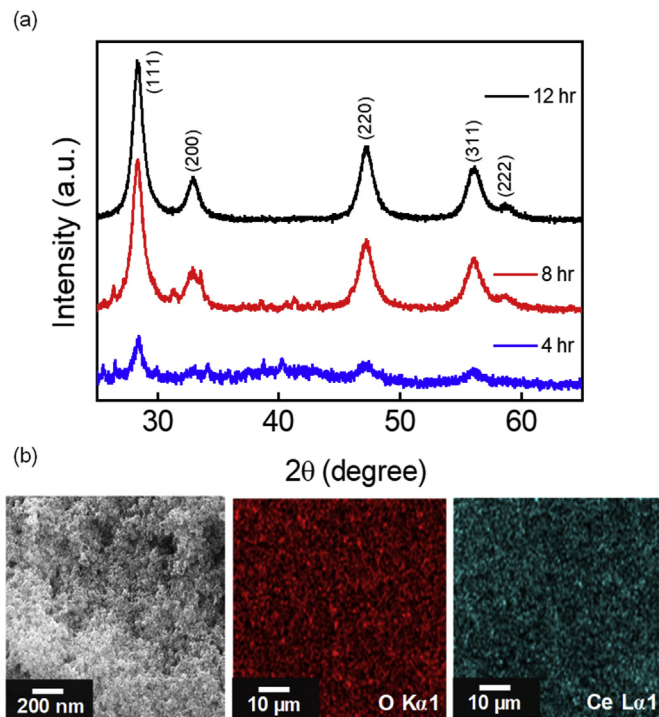The surface hydrophobicity of spin coated CeO$_2$ was studied by

Fig. 2. XRD spectra for CeO$_2$ film which annealed at 200 °C for 4, 8 and 12 h (a) and FE-SEM of CeO$_2$ films with EDS mapping of O and Ce (b).

changing the thickness of CeO$_2$ films. Fig. 3a shows the thickness and WCA as a function of the number of coating cycles used to produce the CeO$_2$ film. As shown in Fig. 3a, film thickness and WCA increase as the number of coating cycles increase. The Si substrate coated with CeO$_2$ NPs over 5 cycles (thickness = ~43 nm), yielded a surface with a WCA of about 90°, indicating that the CeO$_2$ film is highly hydrophobic.

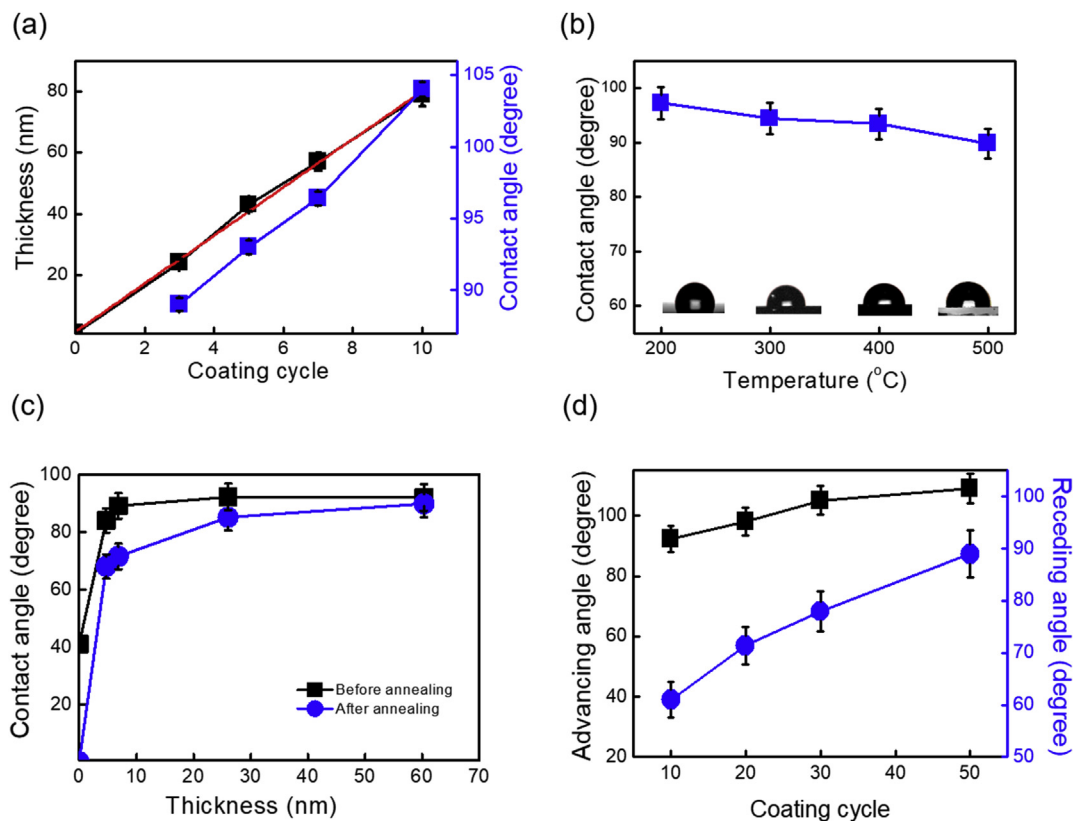To ensure the stability of the CeO$_2$ thin films at high temperatures,

Fig. 3. Film thickness and WCA vs coating cycles (a) WCA at different annealing temperatures (b) WCA as a function of film thickness before and after annealing at 500 °C for 1 h (c) advancing and receding CAs of CeO₂ films with different coating cycles (d).

the thermal stability of the hydrophobic CeO$_2$ films was investigated by annealing them at high temperatures. The WCA of the CeO$_2$ film annealed for 1 h at 200 °C, 300 °C, 400 °C, and 500 °C is shown in Fig. 3b. Results showed that the high temperature annealing treatment did not significantly affect the wetting properties of the CeO$_2$ film. From 200 °C to 500 °C, a decrease of ~5° was observed in the WCA, retaining the hydrophobic properties of the films. Fig. 3c shows the WCA before and after annealing of the CeO$_2$ films with increasing film thicknesses. Before annealing, a 5 nm thick CeO$_2$ film exhibited a WCA of more than 80°. Further, the WCA of the 25 nm thick CeO$_2$ film was more than 90°. Interestingly, the WCA results before and after annealing showed that thicker film is more hydrophobically stable compared to the thinner film. This thickness-dependent hydrophobicity is likely due to a change in film morphology and the formation of defects. After high temperature treatment, there is often a significant mismatch of the thermal expansion coefficient (CTE) between the film and the substrate, and this thermal mismatch leads to the formation of cracks, pits or defects upon annealing [28]. There is a CTE difference of $8.23 \times 10^{-6} \, °/$ C, between CeO$_2$ and Si, such a CTE mismatch between the adjacent layers can lead to the delamination of the film [29], and the inducement of defects in the surface. This ultimately reduces the thermal stability of the thinner films.

Just as film thickness affects hydrophobicity and thermal stability, the effect of thickness on CA hysteresis is studied as well. Advancing and receding CAs of the CeO$_2$ NP films with increasing coating cycles is shown in Fig. 3d. Advancing CA for 10, 20, 30 and 50 cycles is 92, 98, 105, and 109, respectively. Similarly, the receding CA is 60.8, 71.3, 78.3, and 89, respectively. The receding CA increased with increasing cycles to meet the advancing contact angle, thereby decreasing the CA hysteresis. This decrease in CA hysteresis with increasing thickness is probably due to the surface morphological changes that decrease the pinning sites intended for the water droplets to stick to the surface. Lesser number of cycles enables the Wenzel state and the water droplets

can easily stick to the surface; hence, the CA hysteresis becomes large. Upon increasing the number of layers, the Wenzel state can be transformed into the Cassie–Baxter state having low CA hysteresis, which allows the water droplets to easily roll-off from the surface. This trend is in agreement with the previous studies on similar oxide NP coatings [30].

Since spin coating cannot be applied to complex 3D structures, spray coating is a better alternative. Fig. 4a shows the WCA of spray coated CeO$_2$ with different coating cycle durations. Consistently, the change of hydrophobicity in spray coated films, follows the same trend as spin coated films, as shown in Fig. 3a. In addition, the thickness of the spray coated films, like in spin coating, can be changed by the number of coating cycles. Fig. 4b and 4c shows FE-SEM images of films from 30 and 50 coating cycles, respectively. In Fig. 4b, the thickness of the 30 cycle coating was determined to be 102 nm and the WCA was 102°. In Fig. 4c, the thickness of the 50 cycle coating was found to be 161 nm and the WCA indicated a high hydrophobicity of 107°. Importantly, spray coating offers a simple, cheap and scalable coating process, with wide applicability.

Since NP coatings exhibit weak adhesion with substrates due to weak van der Waals forces, there is a dire need to increase the interfacial adhesion between the NPs and the substrate. Thus, experiments were conducted to study the interfacial adhesion and film adhesion properties of the CeO$_2$ films, by including a small percentage of the binder, PAA into the CeO$_2$ NP solution. The purpose of binder addition was to increase the interfacial adhesion of the CeO$_2$ NP coating. The concentration of PAA was first optimized concerning the hydrophobicity of the CeO$_2$ NPs films (Fig. S2, Supporting information). Following homogeneous mixing, the CeO$_2$ NP solution containing PAA, was spray coated onto a Si substrate as described previously. The WCA was measured accordingly to determine the effect of binder inclusion on the hydrophobicity of the resultant CeO$_2$ NP film. Incorporation of 0.05 wt % PAA was found to produce excellent results. WCA values of
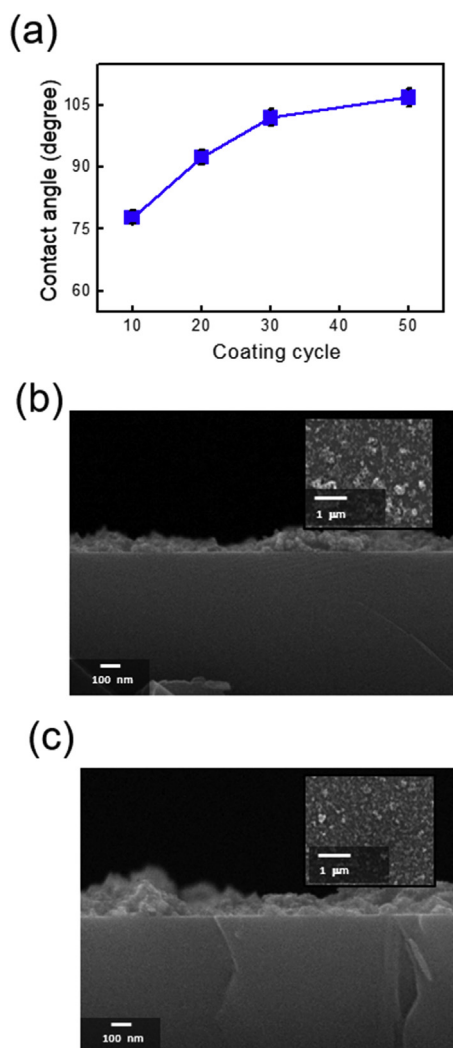
Fig. 4. Spray coating WCA with different coating cycles (a) Top view (inset) and cross-sectional view FESEM images by proceeding 30 cycles (b) and 50 cycles (c) coating.

CeO_2 films with and without PAA, and only PAA as a reference, with increasing numbers of coating cycles are given in Fig. 5a. Interestingly, the WCA remained similar irrespective of the addition of PAA, likely due to its low concentration. To investigate the effect of binder addition, a peel test was employed. Peel force is defined as the force required for separating the materials, which can provide a good estimate of binding strength and interfacial strength. Peel-off behavior for CeO_2 NP films with and without binders is shown in Fig. 5b, as peeling force vs. coating cycles The impact of PAA on the interfacial adhesion was quantitatively assessed via a 3 M tape peeling test. To focus on the cohesion strength among CeO_2 NPs, the peeling test was conducted by stripping 3 M tape attached to the exposed face of a CeO_2 NP film deposited onto a substrate. Peel-off tests for the CeO_2 film (with and without PAA) were conducted at a peel-off angle of 180°. Adhesion measurements showed a significant increase in interfacial force upon binder addition, as shown in Fig. 5b. For CeO_2 NP coatings without PAA, the interfacial adhesion force per unit length was very small and may even be considered negligible, at 3.6, 2.3, and 2.5 gf/mm for 10, 30, and 50 coating cycles, respectively. However, following binder addition, a huge increase in the interfacial strength per unit length of 34, 36, and 61 gf/mm for 10, 30, and 50 coating cycles was observed, respectively. Fig. 5b shows that upon binder inclusion, the films demonstrate excellent interfacial bonding strength as compared to solely CeO_2 films. Typical force per unit length vs. distance plots obtained

from peel-off measurements are presented in Fig. 5c. Fig. 5c shows the peel-off behavior of the CeO_2 films with the binder. As per the figure, the films with binder addition exhibit higher peeling force with the increase in the area under the force–distance curve in comparison to the films without the binder, shown in Fig. 5d. The greater peeling force for the films with the binder, in Fig. 5c, is due to the improvement in the bonding strength between the NPs and substrate surface as well as between the NPs themselves. However, comparatively, in Fig. 5c, negligible force is sufficient to peel-off the film from the substrate, depicting poor adhesion of the NPs with the surface.

The same results were obtained using preliminary adhesion tests via the scotch tape peel-off method, as shown in Fig. S3. CA of the films with and without the binder is shown in Fig. S3a and Fig. S3b, respectively. In Fig. S3a, CA of the solely CeO_2 films, before and after the peel-off tests is shown. CA changed significantly after the peel-off test and the decrease in CA may be attributed to the removal of certain parts of the film. However, films with the binder did not show any significant change in CA, as shown in Fig. S3b, which indicates the improved interfacial adhesion of NPs upon binder addition. Fig. 5f shows CA hysteresis of the CeO_2 NPs films with the binder before and after the peel-off tests. CA hysteresis shows a slight change of ± 2 after the peel-off test. Overall the CA hysteresis showed a decreasing trend with increasing coating cycles. A slight increase in the CA hysteresis upon peel-off test is due to the decrease in advancing CA. This slight change in the CA hysteresis could be due to the slight surface change in the film after the peel-off test.

In addition to the formation of CeO_2 NP films, their thermal stability, interfacial adhesion, hydrophobic properties, and transparency of the films were also considered. Films were coated from 1 cycle to 50 cycles on the glass substrate. Fig. S4a shows the transparency spectra for CeO_2 NPs films with 1–50 cycles in the visible range. According to the spectra, transparency of the films decreased with increasing coating cycles. For 1 cycle, transparency is ~99 %, whereas after 10 coating cycles, transparency decreased to 90 %. Further increase in the coating cycles resulted in further decrease in the transparency level; for 20, 30, and 50 coating cycles, it decreased to 85 %, 83 %, and 75 %, respectively. Fig. S4b shows the transparency measured at a particular wavelength, i.e., 600 nm and plotted as a function of thickness. It further displays the same negative trend of transparency with increasing film thickness. Overall, the films remained transparent even after 50 coating cycles with 161 nm of thickness.

Binder inclusion resulted in a significant increase in the cohesive and adhesive forces between the NPs themselves and between the NPs and the substrate. This is owed to the molecular structure of PAA, as shown in Fig. 5e. Upon drying, the negatively charged carboxylate group of PAA becomes neutral, forming a carboxylic acid group which can form dipole-dipole interactions with CeO_2 particles. This enhances both inter-particle cohesion and particle-to-substrate adhesion [31,32]. Hence, even small amounts of PAA contribute significantly to a substantial loading of CeO_2 particles in the film. We believe that this study can find wide-spread use in many industrial-scale applications. Specifically, a CeO_2-based hydrophobic coating may replace the comparatively expensive Teflon coatings that are used in various cookware. The production of a CeO_2 coating is a much simpler and low-cost process, and produces a favorable non-toxic alternative to Teflon coatings.

4. Conclusions

This study presented a facile, low-cost and low temperature approach to fabricate CeO_2 NPs. The as-prepared CeO_2 NPs were coated onto Si substrates by spin and spray coating processes, to produce thin hydrophobic films. The effect of the coating technique, film thickness and presence of a binder were investigated in relation to film hydrophobicity. To improve the interfacial adhesion between the CeO_2 NPs and a Si substrate, the polymeric binder PAA was incorporated. A drastic decrease in the WCA for the coatings without PAA was observed
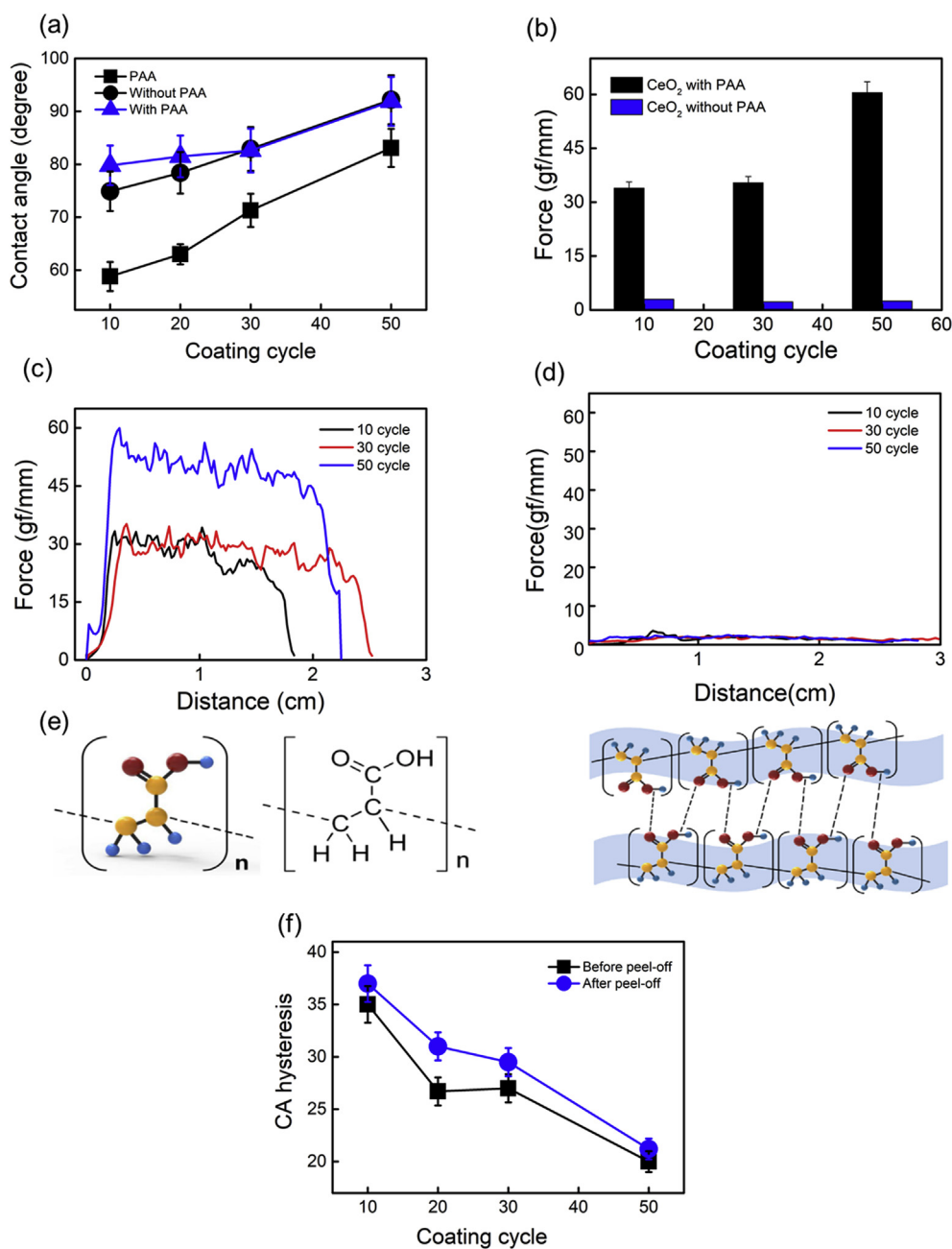
Fig. 5. WCA of CeO_2 coating with and without binder, and only binder (PAA) (a), Adhesion measurements for CeO_2 film by UTM (b) Peeling force per unit length vs. separation distance of tape with the substrate of CeO_2 films with binder (c) and without binder (d) molecular structure of PAA and hydrogen bonding of PAA functional groups within itself (e) CA hysteresis of CeO_2 films before and after peel-off tests (f).

during peel-off tests. However, with PAA, the WCA remained relatively unchanged, predicting better interfacial bonding with the substrate surface. The presence of PAA in the CeO_2 NP coating had no significant effect on its thermal stability at high temperatures. 0.05 wt % of PAA binder was found to be effective as it did not affect the hydrophobicity and significantly increased the interfacial adhesion with the substrate as well. We believe that the fabrication process of CeO_2 NPs with PAA reported herein, is particularly facile and cost-effective, and has the potential to be applied in numerous fields without requiring expensive equipment or chemicals.

Declaration of competing interest

The authors declare that they have no known competing financial interests or personal relationships that could have appeared to

influence the work reported in this paper.

Appendix A. Supplementary data

Supplementary data to this article can be found online at https://doi.org/10.1016/j.ceramint.2020.01.268.

References

[1] J.W. Leem, S. Kim, S.H. Lee, J.A. Rogers, E. Kim, J.S. Yu, Efficiency enhancement of

organic solar cells using hydrophobic antireflective inverted moth-eye nano-patterned PDMS films, Adv. Energy Mater. 4 (2014) 1–7.

[2] D. Quéré, Non-sticking drops, Rep. Prog. Phys. 68 (2005) 2495–2532.

[3] C.B. Contreras, G. Chagas, M.C. Strumia, D.E. Weibel, Permanent superhydrophobic polypropylene nanocomposite coatings by a simple one-step dipping process, Appl. Surf. Sci. 307 (2014) 234–240.

[4] G. Azimi, H.M. Kwon, K.K. Varanasi, Superhydrophobic surfaces by laser ablation of rare-earth oxide ceramics, MRS Commun. 4 (2014) 95–99.

[5] S. Khan, G. Azimi, B. Yildiz, K.K. Varanasi, Role of surface oxygen-to-metal ratio on the wettability of rare- earth oxides, Appl. Phys. Lett. 106 (2015) 061601.

[6] D. Bonn, J. Eggers, J. Indekeu, J. Meunier, E. Rolley, Wetting and spreading, Rev. Mod. Phys. 81 (2009) 739–805.

[7] G. Azimi, R. Dhiman, H.M. Kwon, A.T. Paxson, K.K. Varanasi, Hydrophobicity of rare-earth oxide ceramics, Nat. Mater. 12 (2013) 315–320.

[8] G. Adachi, N. Imanaka, Z.C. Kang (Eds.), Binary Rare Earth Oxides, vol. 4, Springer Science & Business Media, 2004.

[9] N.E. Topp, The Chemistry of the Rare-Earth Elements vol. 4, Elsevier Pub. Co., 1965.

[10] L. Xu, R.G. Karunakaran, J. Guo, S. Yang, Transparent, superhydrophobic surfaces from one-step spin coating of hydrophobic nanoparticles, ACS Appl. Mater. Interfaces 4 (2012) 1118–1125.

[11] R. Fiala, A. Figueroba, A. Bruix, M. Vaclavu, A. Rednyk, I. Khalakhan, M. Vorokhta, J. Lavkova, F. Illas, V. Potin, High efficiency of Pt^{2+}- CeO_2 novel thin film catalyst as anode for proton exchange membrane fuel cells, Appl. Catal. B Environ. 197 (2016) 262–270.

[12] I.K. Oh, K. Kim, Z. Lee, K.Y. Ko, C.W. Lee, S.J. Lee, J.M. Myung, C. Lansalot-Matras, W. Noh, C. Dussarrat, Hydrophobicity of rare earth oxides grown by atomic layer deposition, Chem. Mater. 27 (2015) 148–156.

[13] A.P. Milanov, R.A. Fischer, A. Devi, Synthesis, characterization, and thermal properties of homoleptic rare-earth guanidinates: promising precursors for MOCVD and ALD of rare-earth oxide thin films, Inorg. Chem. 47 (2008) 11405–11416.

[14] L. Hu, X. Song, D. Jin, C. Xing, X. Shan, X. Zhao, P. Xiao, A robust quasi-superhydrophobic ceria coating prepared using air-plasma spraying, J. Am. Ceram. Soc. 102 (2019) 1386–1393.

[15] M. Bai, H. Kazi, X. Zhang, J. Liu, T. Hussain, Robust hydrophobic surfaces from suspension HVOF thermal sprayed rare-earth oxide ceramics coatings, Sci. Rep. 8 (2018) 6973.

[16] L. Martínez, E.D. Roman, J.L. De Segovia, S. Poupard, J. Creus, F. Pedraza, Surface study of cerium oxide based coatings obtained by cathodic electrodeposition on zinc, Appl. Surf. Sci. 257 (2011) 6202–6207.

[17] I.S. Bayer, On the durability and wear resistance of transparent superhydrophobic coatings, Coatings 7 (2017) 12.

[18] T. Suzuki, I. Kosacki, H.U. Anderson, Microstructure–electrical conductivity relationships in nanocrystalline ceria thin films, Solid State Ionics 151 (2002) 111–121.

[19] A. Matsuzaki, M. Yamashita, N. Hara, Effect of pretreatment film composition on adhesion of organic film on zinc coated steel sheet, Mater. Trans. (2010) 1008171152-1008171152.

[20] V.P. Nguyen, S. Moon, Effects of surface pretreatment on deposition and adhesion of electrophoretic paint on AZ31 Mg Alloy, J. Kor. Inst. Surf. Eng. 50 (2017) 72–84.

[21] K.G. Kim, S.Y. Kim, Increase in interfacial adhesion and electrochemical charge Storage capacity of polypyrrole on Au electrodes using polyethyleneimine, Sci. Rep. 9 (2019) 2169.

[22] R. Guo, S. Zhang, H. Ying, W. Yang, J. Wang, W.Q. Han, New, effective, and low-cost dual-functional binder for porous silicon anodes in lithium-ion batteries, ACS Appl. Mater. Interfaces 11 (2019) 14051–14058.

[23] K. Lee, J. Lee, S. Choi, K. Char, J.W. Choi, Thiol–ene click reaction for fine polarity tuning of polymeric binders in solution-processed all-solid-state batteries, ACS Energy Lett. 4 (2018) 94–101.

[24] Z. Burton, B. Bhushan, Hydrophobicity, adhesion, and friction properties of nano-patterned polymers and scale dependence for micro-and nanoelectromechanical systems, Nano Lett. 5 (2005) 1607–1613.

[25] A. Magasinski, B. Zdyrko, I.B. Kovalenko, B.J. Hertzberg, R. Burtovyy, C.F. Huebner, T.F. Fuller, I. Luzinov, G. Yushin, Toward efficient binders for Li-ion battery Si-based anodes: polyacrylic acid, ACS Appl. Mater. Interfaces 2 (2010) 3004–3010.

[26] L. Wei, Z. Hou, High performance polymer binders inspired by chemical finishing of textiles for silicon anodes in lithium ion batteries, J. Mater. Chem. 5 (2017) 22156–22162.

[27] D. Quéré, Wetting and roughness, Annu. Rev. Mater. Res. 38 (2008) 71–99.

[28] W. Fang, C.Y. Lo, On the thermal expansion coefficients of thin films, Sensor Actuator A Phys. 84 (2000) 310–314.

[29] J.H. Kim, K.L. Jang, K. Ahn, T. Yoon, T.L. Lee, T.S. Kim, Thermal expansion behavior of thin films expanding freely on water surface, Sci. Rep. 9 (2019).

[30] L. Cao, D. Gao, Transparent superhydrophobic and highly oleophobic coatings, Faraday Discuss 146 (2010) 57–65.

[31] S. Luangkularb, S. Prombanpong, V. Tangwarodomnukun, Material consumption and dry film thickness in spray coating process, Procedia CIRP 17 (2014) 789–794.

[32] R. Joksimovic, S. Prevost, R. Schweins, M.S. Appavou, M. Gradzielski, Interactions of silica nanoparticles with poly(ethylene oxide) and poly(acrylic acid): effect of the polymer molecular weight and of the surface charge, J. Colloid Interface Sci. 394 (2013) 85–93.